

Invariant manifolds of L_3 and horseshoe motion in the restricted three-body problem

Esther Barrabés⁽¹⁾ and Mercè Ollé⁽²⁾

2nd June 2006

- (1) Dept. Informàtica i Matemàtica Aplicada, Universitat de Girona, Avd. Lluís Santaló s/n, 17071 Girona, Spain. E-mail: barrabes@ima.udg.es
- (2) Dept. de Matemàtica Aplicada I, ETSEIB, Universitat Politècnica de Catalunya, Diagonal 647, 08028 Barcelona, Spain. E-mail: merce.olle@upc.edu

Abstract

In this paper, we consider horseshoe motion in the planar restricted three-body problem. On one hand, we deal with the families of horseshoe periodic orbits (which surround three equilibrium points called L_3 , L_4 and L_5), when the mass parameter μ is positive and small; we describe the structure of such families from the two-body problem ($\mu = 0$). On the other hand, the region of existence of horseshoe periodic orbits for any value of $\mu \in (0, 1/2]$ implies the understanding of the behaviour of the invariant manifolds of L_3 . So, a systematic analysis of such manifolds is carried out. As well the implications on the number of homoclinic connections to L_3 , and on the *simple* infinite and *double* infinite period homoclinic phenomena are also analysed. Finally, the relationship between the horseshoe homoclinic orbits and the horseshoe periodic orbits are considered in detail.

Keywords: periodic orbits, invariant stable and unstable manifolds, homoclinic orbits, restricted problem.

1 Introduction

Over the past decades the interest in horseshoe periodic orbits (roughly speaking banana-shaped orbits) arose when modelling the motion of co-orbital satellites, the most famous being Saturn's co-orbital satellites Janus (1980S1) and Epimetheus (1980S3), whose existence was confirmed by Voyager flights to Saturn in 1981 (see [7], [8], [17] and references therein). More recently, several near-Earth asteroids have been found to move on horseshoe orbits (see [5] and [3]).

The horseshoe motion and the dynamics of co-orbital satellites have been analysed both analytically and numerically using the three-body context. In the framework of singular perturbation theory the motion of co-orbital satellites may be approximated by two independent solutions of a two-body problem when they are far apart. However, this approximation breaks down when the distance of the two satellites becomes small, and a different two-body problem must be used instead. The complete description of the motion requires the matching of both solutions (see [22] and [24]). Cors and Hall [6] studied the same problem by introducing small parameters to the three-body equations, truncating higher order terms and deriving dynamical information from the resulting equations. From a numerical point of view, horseshoe periodic orbits have been explored as invariant objects using Hill's problem (see [20]), the *planar* restricted three-body problem – RTBP– (as a simple model to describe Saturn's co-orbital motion with the mass parameter $\mu = 3.5 \times 10^{-9}$, see [16] and [17]) and the *spatial* RTBP (where some families of horseshoe periodic orbits were computed, see [1]).

In this paper we consider the planar RTBP. It is known that this problem has five equilibrium points (in a rotating system of reference) called L_i , $i = 1, \dots, 5$ and a first integral called the Jacobi integral. We will denote by C the constant value of the Jacobi integral along a solution. Throughout the paper we study some open questions concerning horseshoe periodic orbits (HPO) not answered in previous papers. We focus our attention on periodic symmetric solutions of the RTBP in a rotating system. In this context, HPOs are orbits that surround the equilibrium points L_3 , L_4 and L_5 , and have two orthogonal crossings with the horizontal synodical axis (see Figures 3, 7 and 8).

Our contribution in this paper is threefold:

- (i) for a value of μ fixed and small, and for a *big interval* of values of the Jacobi constant C , the understanding of the diagram of *continuous families* of HPOs follows from the families of periodic orbits obtained from rotating circular and elliptical orbits in the $\mu = 0$ case (in [17] only a mechanism to generate one set of *isolated* HPOs for a *fixed* value of the Jacobi constant was given). From now on we call such families for $\mu = 0$ *generating families of HPOs* and we give their analytical expression.
- (ii) Many properties concerning the evolution of the families, for $\mu > 0$ and small, as well as the shape of the HPOs within a family, are now easily explained from the generating families of HPOs. The diagram of the characteristic curves of the families of HPOs is computed for $\mu = 0.0001$ and we remark on the similarities and differences between this diagram and the corresponding one for $\mu = 0$.

- (iii) However, the continuation of this diagram when varying $\mu > 0$ is not straight forward. This is mainly due to the existence of the stable and unstable invariant manifolds of the collinear equilibrium point L_3 . In particular the behaviour of such manifolds for $C_3 = C(L_3)$ and the existence of a finite or infinite number of HPOs for this value C_3 are analysed in order to understand how the diagram of families of HPOs evolves when increasing μ . Finally, we study the existence and location of horseshoe periodic orbits and horseshoe homoclinic orbits to L_3 for any value of $\mu \in (0, 1/2]$. Since the invariant manifolds of L_3 play a key role as a mechanism to generate HPOs, we have done a detailed exploration of the behaviour of these manifolds when increasing μ from 0 onwards. In particular, we study the existence of homoclinic horseshoe orbits to L_3 (that is, an orbit that tends to L_3 in backward and forward time) when varying μ . For each homoclinic orbit there is an infinity of HPOs tending to it. Furthermore, we observe that the set of values of μ for which *simple* homoclinic orbits exist, is a sequence tending to zero. And, tending to each *simple* isolated homoclinic orbit, a double sequence of *double* homoclinic orbits can be obtained. (See Section 4 for the explicit definition of simple and double homoclinic orbits.)

As a final remark, we must point out that not only L_3 is important in the horseshoe dynamics, but also the other collinear equilibrium points L_1 and L_2 , and the equilateral ones, L_4 and L_5 (as well as the periodic orbits around them and their associated invariant manifolds), are also involved. We show some examples.

In Section 2 we briefly recall the RTBP. Items (i) and (ii) are developed in Section 3 and item (iii) is done in Section 4.

2 The restricted three-body problem

Let us consider a system of three bodies in an inertial (also called sidereal) reference system. Two bodies, called big and small primaries of masses $1 - \mu$ and μ , $\mu \in (0, 1/2]$, (in suitable units), are describing circular orbits about their common centre of mass (the origin of coordinates) in a plane. The third body is a particle of infinitesimal mass which moves under the gravitational effect of the primaries but has negligible effect on their motion. The problem of the description of the motion of the particle is known as the circular restricted three-body problem (RTBP). With suitable units, such as the mean motion of the primaries is the unity, the equations of motion in a rotating (also called synodical) system of coordinates, where the big and small primaries remain fixed at positions $(\mu, 0)$ and $(\mu - 1, 0)$ respectively, are (see Szebehely [23])

$$\begin{aligned} x'' - 2y' &= \frac{\partial \Omega}{\partial x}, \\ y'' + 2x' &= \frac{\partial \Omega}{\partial y}, \end{aligned} \tag{1}$$

where

$$\Omega(x, y) = \frac{1}{2}(x^2 + y^2) + \frac{1 - \mu}{r_1} + \frac{\mu}{r_2} + \frac{1}{2}\mu(1 - \mu),$$

$r_1^2 = (x - \mu)^2 + y^2$ and $r_2^2 = (x - \mu + 1)^2 + y^2$ are the distances between the particle and the big and small primaries respectively, and \prime stands for d/dt .

It is well known that these equations have the so called Jacobi first integral

$$x'^2 + y'^2 = 2\Omega(x, y) - C. \quad (2)$$

It will be necessary to take into account the regions in the (x, y) plane where the motion of the particle is possible. These regions are bounded by the zero velocity curves (ZVC) given by the equation

$$2\Omega(x, y) - C = 0.$$

obtained from (2) (see Fig. 1).

Finally, Equations(1) satisfy the symmetry

$$(x, y, x', y', t) \rightarrow (x, -y, -x', y', -t). \quad (3)$$

Using this symmetry, it is well known that any solution with two orthogonal crossings with the horizontal axis becomes symmetric, with respect to the x axis, and periodic. We can consider that the orthogonal crossings occur at epochs $t = 0$ and $t = T/2$, with T being the period. Given a periodic orbit, we denote its initial conditions (at $t = 0$) by $(x_0, 0, 0, y'_0)$ (or in short (x_0, y'_0)) and the final conditions (at $t = T/2$) by $(x_f, 0, 0, y'_f)$ ((x_f, y'_f)).

There exist 5 equilibrium points: the collinear points, L_1 , L_2 and L_3 , with positions $(x_i, 0)$, for $i = 1, 2, 3$, and the equilateral ones, L_4 and L_5 , located at $(\mu - 1/2, \pm\sqrt{3}/2)$. If one computes the value of the Jacobi constant at the equilibrium points $C_i = C(L_i)$ for any value of $\mu \in (0, 1/2)$, one has (see [23])

$$3 = C_4 = C_5 < C_3 \leq C_1 < C_2,$$

and $C_3 = C_1$ for $\mu = 1/2$. Along the paper, the point L_3 and its invariant manifolds will play a key role. We briefly recall that, according to the eigenvalues of the Jacobian matrix of the vector field at L_3 , the collinear point is saddle-centre type. That is, the eigenvalues are $\lambda_1 = a > 0$, $\lambda_2 = -a$ and $\lambda_{3,4} = \pm bi$, $b \in \mathbb{R}$ (this is also true for the other collinear points L_1 and L_2). In particular, L_3 has one-dimensional unstable and stable manifolds associated to the saddle. In particular, an eigenvalue v associated with the eigenvalue λ_1 (respectively λ_2) gives the tangent direction of the unstable (stable) manifold. Each branch of the unstable (resp. stable) manifold tends asymptotically to the equilibrium point in backward (forward) time. We shall distinguish between the two branches of the unstable (or stable) manifold according to v or $-v$, which will be denoted by $W_{L_3}^{u,1}$, $W_{L_3}^{u,2}$ for the unstable manifold of L_3 and by $W_{L_3}^{s,1}$, $W_{L_3}^{s,2}$ for the stable one. Actually only $W_{L_3}^{u,1}$ and $W_{L_3}^{u,2}$ have to be computed since $W_{L_3}^{s,1}$ and $W_{L_3}^{s,2}$ can be obtained from the symmetry (3).

We also recall that if one branch of the invariant unstable manifold crosses orthogonally the x axis (that is, $y = x' = 0$), due to the symmetry (3), the branch coincides with one branch of the stable manifold at this point, giving rise to a homoclinic orbit. This orbit tends asymptotically, in forward and backward time, to L_3 .

3 Families of planar horseshoe periodic orbits

According to [17], a planar *horseshoe* periodic orbit will be a periodic solution of the RTBP in which the particle follows a path which surrounds only the equilibrium points L_3 , L_4 and L_5 and has two orthogonal crossings with the x axis. This implies that the HPOs considered are symmetric with respect to the horizontal axis. For greater clarity, some included plots of the periodic orbits only show a half-period of the motion (for $t \in [0, T/2]$, see for example, Figures 3 right, 7 and 8) and the dotted line represents the horizontal axis in the synodical reference system where the primaries are located.

An initial question concerns the suitable region in the plane (x, y) to find horseshoe motion. It is clear from the zero velocity curves (see Figure 1) that the equilibrium points L_i , $i = 1, 2, 3, 4, 5$, play a role here and that horseshoe motion is only possible for $C < C_1$ (see [23] for the expansions in μ of x_i and C_i , for $i = 1, 2, 3$). Thus, we will begin our numerical explorations by using values of the Jacobi constant between C_3 and C_1 .

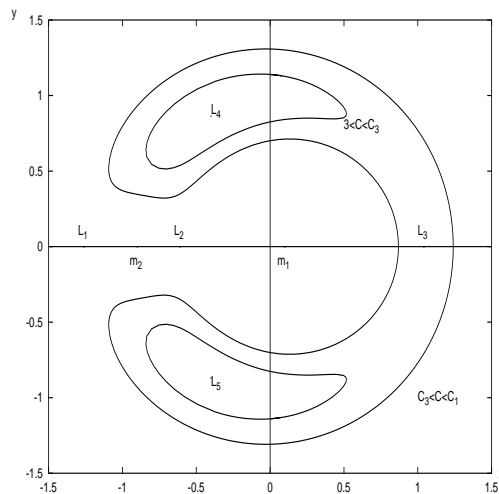


Figure 1: Zero velocity curves for $\mu > 0$. The motion is possible outside the region enclosed by the ZVC. Horseshoe motion takes place for values $C < C_1$.

Given a value of $\mu > 0$ and small, a second question will refer to a mechanism that explains the existence of HPOs from the $\mu = 0$ case. In this sense, for $\mu \neq 0$ and for any HPO when $t \in [0, T/2]$, we will distinguish between the *outer* solution, the piece of the HPO from $t = 0$ to the returning point (close to the small primary), and the *inner* solution from the returning point to $t = T/2$ (analogously for $t \in [T/2, T]$). The outer and inner solutions can be approximated by two different solutions of the rotating two-body problem when the infinitesimal mass is far from the small primary. In Figure 2 we

show two HPOs, for $\mu = 0.0001$, and the corresponding approximating rotating circular orbits (left) and rotating elliptical ones (right), for $\mu = 0$. In Subsection 3.1, we study the families of periodic orbits of the two-body problem that give the outer and inner approximations of the HPOs. We call such families *generating families* of the HPOs for $\mu = 0$. We also give analytic expressions that describe the families and the corresponding diagram in suitable variables.

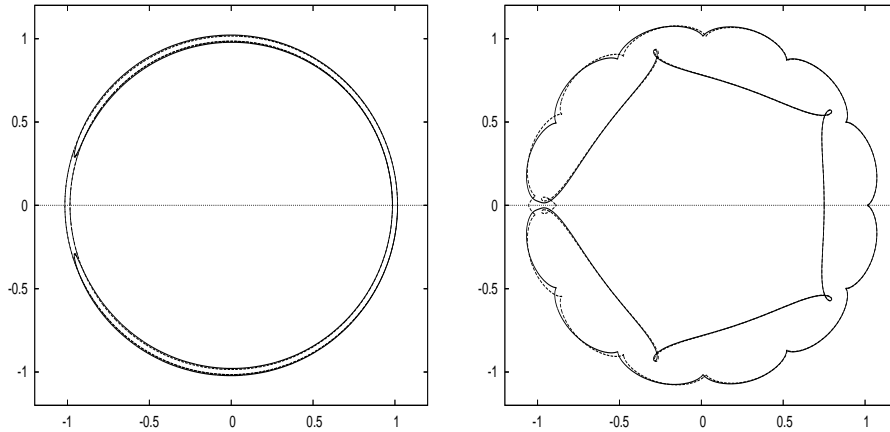


Figure 2: A whole HPO (continuous line) for $\mu = 10^{-4}$ and the two-body orbits (discontinuous line) for $\mu = 0$ approximating the outer and inner solutions.

Next, we consider the families of HPOs for $\mu > 0$ and small (Subsection 3.2). First, a method of numerical computation of such families is given. Secondly, we describe the diagram of characteristic curves (curves such that each point characterises an HPO) for a specific value of μ (0.0001) and we compare it with the diagram of continuous families of rotating ellipses and circular orbits for $\mu = 0$.

Finally, it is natural to consider the continuation of this diagram for increasing values of μ . However, this is not a straightforward task. The explanation comes from the behaviour of the invariant manifolds of the equilibrium point L_3 . In Subsection 3.3, we observe that the loops that appear in the (x, y) -projection of the invariant manifolds and the existence of homoclinic orbits to L_3 (orbits that tend to this point in backward and forward time) play an important role in order to describe the continuation of these diagrams.

3.1 Generating families of HPOs for $\mu = 0$

When $\mu = 0$ we consider the sidereal orbits described by the particle around the big primary located at the origin, as natural candidates to approximate the outer and inner solutions of a horseshoe orbit. We distinguish between a circular sidereal orbit (which becomes also a synodical circular one) or a synodical orbit coming from a rotating sidereal ellipse. In order to characterise the families of sidereal circular and elliptical orbits, we consider the well known relation

$$\frac{C}{2} + h = M, \quad (4)$$

with C the Jacobi constant, h the energy and M the angular momentum with sign: positive for direct orbits and negative for retrograde ones. As $M = \pm\sqrt{a(1-e^2)}$ and $h = -1/2a$ (a, e being the semimajor axis and the eccentricity) we obtain

$$\frac{C}{2} - \frac{1}{2a} = \pm\sqrt{a(1-e^2)}, \quad (5)$$

or equivalently

$$e^2 + \frac{1}{4a} \left(C - \frac{1}{a}\right)^2 = 1. \quad (6)$$

First, we consider the circular orbits. Substituting $e = 0$ in Equation (5), we obtain

$$C = \frac{1}{a} \pm 2\sqrt{a} \quad (7)$$

with the plus sign (the $l-i$ families in the Strömberg's notation, see for example [12]) for sidereal direct orbits and the minus sign (the $h-m$ families) for sidereal retrograde ones. Each such orbit will have as initial synodical position the point $(x, 0)$, with $x = a$ satisfying Equation (7). In Figure 3, both curves are represented, as well as the ZVC obtained from Equation (2) considering $\mu = 0$, i.e. $x^2 + 1/x = C$.

In order to approximate an HPO, we are interested in the two circular orbits of families $l-i$ close to the ZVC, for a value of $C > 3$ fixed (see Figure 3). Two such circular orbits will approximate the outer and inner solutions of an HPO for small $\mu > 0$ (see Figure 2 left). Because of this, this family is called the generating (or also approximating) family of circular orbits.

It should be noted that for any sidereal orbit we have, from Kepler's third law, that $n^2 a^3 = 1$, where n and $n-1$ are the sidereal and synodical mean motions respectively. If $n < 0$, the orbit is retrograde in both reference systems, while for $0 < n < 1$ ($a > 1$) the orbit is sidereal direct but synodical retrograde and for $n > 1$ ($a < 1$) direct in both systems. Therefore, the outer and inner solutions of an HPO are approximated by a retrograde and a direct synodical circular solution respectively.

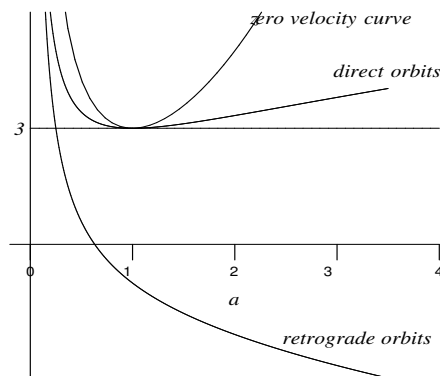


Figure 3: Plane (x, C) ; the ZVC and the two families of sidereal circular orbits (of radius $x = a$) of the problem of two bodies given by equation (7).

Circular orbits are always symmetric and periodic in both sidereal and synodical reference systems. However, in order for a rotating ellipse to be symmetric and periodic in the synodical system, a rational mean motion $n = Q/P$ is necessary (or equivalently the semimajor axis a has to verify the condition $a = (P/Q)^{2/3}$, for $P, Q \in \mathbb{N}$ relatively primes), and the two orthogonal crossings in the synodical x axis must take place at a pericentre or an apocentre of the sidereal orbit.

So, let $x > 0$ be the value of the synodical x coordinate of the initial orthogonal crossing. Then $x = a(1 + e)$ if it is at an apocentre or $x = a(1 - e)$ at a pericentre. In both cases, $e^2 = \frac{(x-a)^2}{a^2}$ and Equation (6) becomes

$$\frac{(x-a)^2}{a^2} + \frac{1}{4a} \left(C - \frac{1}{a} \right)^2 = 1, \quad (8)$$

which gives a curve the (x, C) plane that, for a fixed value of a , is an ellipse itself with centre $(a, 1/a)$ and semimajor axis a and $2\sqrt{a}$. So, for fixed a , the points in the ellipse of Equation (8) give a family of elliptical orbits and each of these points represents an elliptic orbit with semimajor axis a and eccentricity $e = |x - a|/a$ (see Figure 4 left). If $x > a$ (respectively $x < a$) the orthogonal crossing takes place at the apocentre (resp. pericentre). When $x = a$, we have a circular orbit ($e = 0$), and for $x = 0$ or $x = 2a$, we get a degenerate ellipse ($e = 1$) (see Figure 4 right). Also, from Equation (5) and for a fixed value of a , we distinguish between direct and retrograde orbits according to the value of the Jacobi constant:

$$C \in \left(\frac{1}{a} - 2\sqrt{a}, \frac{1}{a} \right) \quad \text{sidereal retrograde orbits,}$$

$$C \in \left(\frac{1}{a}, \frac{1}{a} + 2\sqrt{a} \right) \quad \text{sidereal direct ones.}$$

Both intervals correspond to the upper and lower semiellipses of the associated ellipse (labelled by a). Again if $a < 1$ (respectively $a > 1$) the orbit becomes synodical direct (retrograde).

We also note that for any fixed value of a , the corresponding family of elliptical orbits given by Equation (8) intersects the family of circular orbits at two points (see Figure 4 left): $(a, \frac{1}{a} + 2\sqrt{a})$ corresponding to a circular orbit and (x, C) that corresponds both to a circular orbit with radius x and to an ellipse with $x = a(1 + e)$ or $x = a(1 - e)$. A deeper analysis shows that, if $a < 1$ the initial orthogonal crossing x of the ellipse is at an apocentre while for $a > 1$ the initial x is at a pericentre. Furthermore, for $a < 2^{-5/3}$ the orbit is sidereal retrograde whereas for $2^{-5/3} < a$ the orbit is sidereal direct. So we have two different orbits (circular and elliptic) with the same initial condition $(x, 0)$, but with different sign in the initial velocity y' (see also Subsection 3.2 for details). We note that the sign of the velocity does not determine the sense of the synodical orbit: the velocity may be negative for a direct synodical orbit, due to the existence of loops (see for example Figures 7 and 8).

As reasoned above, the solutions of Equation (8) will be called the generating families of rotating ellipses. Finally, we remark that Equations (7) and (8) may be regarded as the equations of the characteristic curves of families of symmetrical periodic orbits for $\mu = 0$.

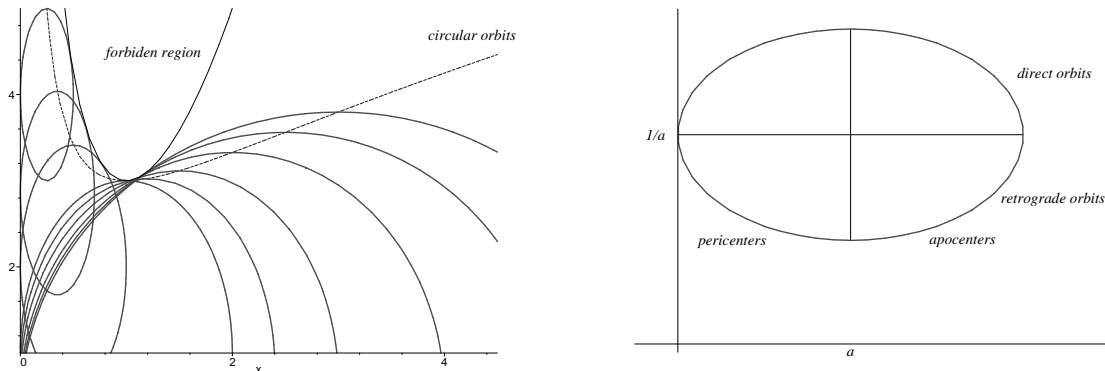


Figure 4: Left. Families of sidereal elliptical orbits in the plane (x, C) . Right. One family given by Equation (8) with a fixed a . Points $(a, 1/a \pm 2\sqrt{a})$ represent circular orbits.

For a fixed a , a point of the curve in the plane (x, C) gives rise to the synodical initial condition $(x, 0, 0, y')$, with $y' = \pm v - x$ (plus or minus sign if the sidereal orbit is direct or retrograde respectively), $v = \sqrt{\frac{1 \pm e}{a(1 \mp e)}}$, and $x = a(1 \mp e)$, where the up (down) sign is taken if the particle is at the pericentre (apocentre). Such characteristic curves will be meaningful when studying the HPOs for small $\mu > 0$ in Subsection 3.2.

3.2 Families of HPOs for $\mu > 0$ and small

The aim of this Subsection is to compare the diagram of characteristic curves of families of HPOs for $\mu > 0$ and small with the generating families for $\mu = 0$, and to derive some properties of the families for $\mu > 0$.

Thus, in this Subsection, we fix a value of $\mu > 0$ and small, for example $\mu = 10^{-4}$. We want to obtain, numerically, families of symmetrical horseshoe periodic orbits. Each periodic orbit is completely determined by its initial condition (x_0, y'_0) , and a family can be represented by the set of the initial conditions of its periodic orbits. Thus, each family can be represented by a curve (characteristic curve) for example in the (x_0, y'_0) -plane, or in the (x_0, C) -plane, C obtained from Equation (2). The last, being our choice.

In order to compute the families of HPOs, we take into account that a family of periodic orbits with initial conditions $(x_0, 0, 0, y'_0)$ is defined implicitly by the equation

$$x'(T/2, x_0, y'_0) = 0$$

where $T = T(x_0, y'_0)$ is given by the Poincaré section $y(T/2, x_0, y'_0) = 0$. The numerical continuation of the family has been done using the arc step method which we will outline. A family of periodic orbits is regarded as a curve parameterised by the arc parameter s , that is,

$$p(s) = (x_0(s), y'_0(s))$$

such that $x'_f(p(s)) = 0$, where x'_f stands for the value of x' when the first (or k -th) crossing with the x axis takes place. Using the fact that the curve $p(s)$ satisfies a suitable system

of differential equations, we predict the successive points on the curve by a (low) order Adams-Bashforth method and we refine them by using a modified Newton's method (see for example [1], [2] or [21] for details).

Of course an initial point (seed) of each family must be taken. To obtain it, we fix a value of C , and for any value x_0 (greater than $x_3 = x(L_3)$ if $C \geq C_3$) we integrate the equations of motion until the first (or k -th) crossing with the horizontal axis is reached. At this point, $y_f = 0$, but in general $x'_f \neq 0$ (is not an orthogonal crossing). Then we consider x'_f as a function of the initial x_0 . In Figure 10, this function is shown for $C = C_3$ and different values of μ (see also Subsection 3.3 and [17] for more details). Each value x_0 for which $x'_f = 0$ represents a periodic orbit, so for a fixed value of C we obtain a discrete number of HPOs, and for each one we can follow its family using the above mentioned method. We show in Figure 5, and for $\mu = 0.0001$, some of the characteristic curves of the families of HPOs computed in the (x_0, C) plane (C obtained from x_0 and y'_0). Only the initial conditions of horseshoe orbits with two crossings (just the orthogonal ones) with the horizontal axis have been computed, so the plot of the branches stops when the HPO has more than two crossings. Also, the discrete set of initial conditions of HPOs computed for the fixed value $C = 3.00019$ (the points shown with crosses), as well as the Lyapunov family around L_3 (periodic orbits around the equilibrium point, which have no horseshoe shape), and the ZVC (the continuous line curve on the left in the Figure) given by equation

$$C = \frac{2(1 - \mu)}{x_0 - \mu} + \frac{2\mu}{x_0 + 1 - \mu} + \mu(1 - \mu) + x_0^2,$$

are shown in this Figure.

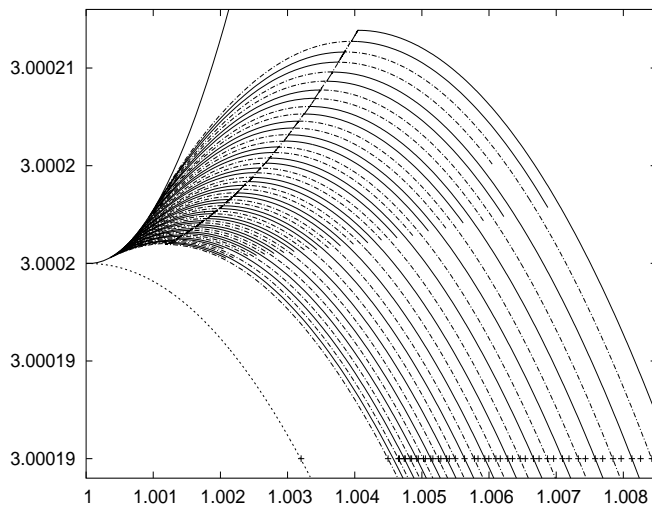


Figure 5: Characteristic curves of some families of HPOs in the (x_0, C) plane. The cross points correspond to the periodic orbits computed for the fixed value $C = 3.00019$. The separated dotted curve at the bottom left corresponds to the Lyapunov family of periodic (not horseshoe) orbits around L_3 . See the text for more details.

At this point we want to comment on some properties concerning the evolution of the

families, and to compare the diagram of the characteristic curves with the diagram of generating families for $\mu = 0$:

- (i) We have considered the eccentricity (which is not constant along an HPO) at the initial condition of an HPO and we think of this value of e as the eccentricity of the outer approximation. It is proved in [1] that the points (x_0, C) for which the outer approximation with the same initial conditions has eccentricity zero satisfy the equation

$$C = \frac{2(1 - \mu)}{x_0 - \mu} + \frac{2\mu}{x_0 + 1 - \mu} + \mu(1 - \mu) + 2\sqrt{x_0} - \frac{1}{x_0}. \quad (9)$$

This is the dashed line in Figure 6 (called skeleton in [1]) and corresponds to the generating family $l - i$ of circular orbits for $\mu = 0$ (see Figure 4 left).

- (ii) Each continuous family reaches a maximum value of C , denoted by C_m . We distinguish between two kinds of families, either the family ‘crosses’ the skeleton or it does not (see Figure 6). In any case we can consider both branches in each curve: on the left and right sides of the skeleton if it is crossed by the characteristic curve, or on the same side if it is not. In any case, the two branches of the family are very close to one generating family (for $\mu = 0$) which is different for each branch. That is, for $\mu > 0$ and small, the generating families that approach each branch do not coincide and then, the values of the semimajor axis a and a' associated to each generating family are different. This means that the outer solution of orbits belonging to the same family but to a different branch can be approximated by ellipses with different semimajor axis.

The same property can be derived for the inner solution of orbits belonging to the same family but to a different branch. We can consider the characteristic curves of the families by taking into account the points (x_f, C) , x_f being the x position at $t = T/2$ (see Figure 6, where the dotted curves correspond to the points (x_f, C) for two particular families labelled as A and C). The same observation in this case can be made: each curve has two branches which can be approximated by two different generating families for $\mu = 0$ (although in the aforementioned Figure they cannot be appreciated).

- (iii) In particular, let us consider one family of HPOs and one branch of the family. As the branch can be approximated by one generating family for $\mu = 0$, the outer solution of each HPO is near a rotating ellipse with the *same* semimajor axis a for all of the orbits of the family, but with different eccentricity. As C decreases, the eccentricity varies from 0 onwards along the branch. As specific examples, we consider families A and C (see Figure 6), and we plot the (x, y) projection of some orbits belonging to the families in Figures 7 and 8: the subplots (1), (2) and (3) correspond to orbits with initial conditions in the left branch of each family, and (4), (5) and (6) correspond to orbits in the right branch. We can see how the increase of the eccentricity is translated to bigger loops and therefore to an increasing number of

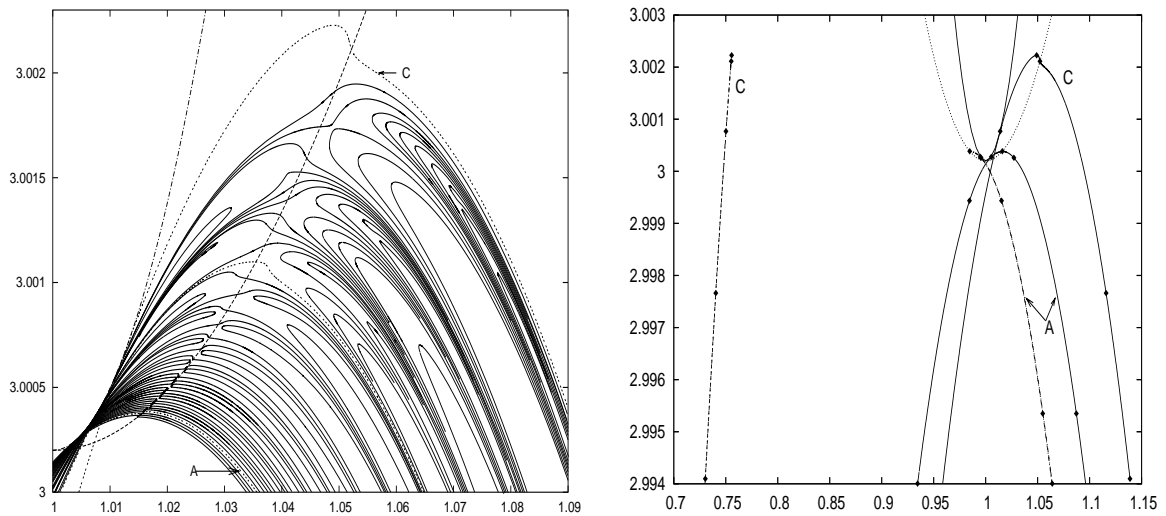


Figure 6: Left: characteristic curves (x_0, C) of some families of HPOs for $\mu = 0.0001$. The dashed-dotted line on the right represents the ZVC, and the dashed line crossing all the families is the skeleton curve given by Eq. 9. Right: characteristic curves (x_0, C) (continuous line) and (x_f, C) (dashed line) of families A and C. The points indicated on each curve correspond to the orbits, with increasing x_0 , shown in Fig. 7 and 8.

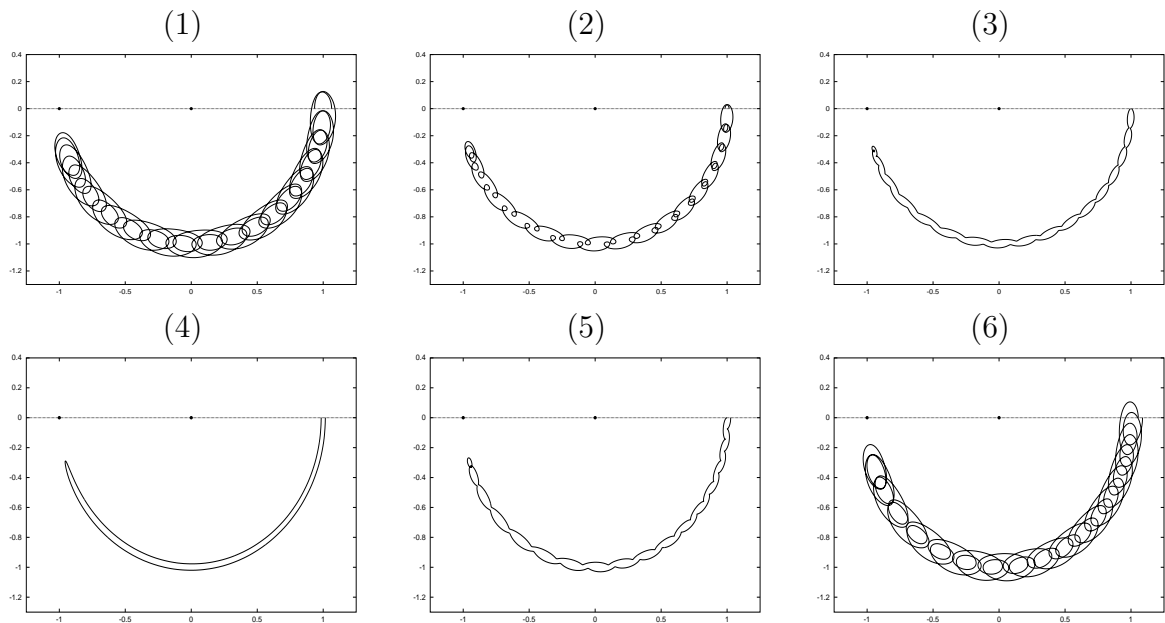
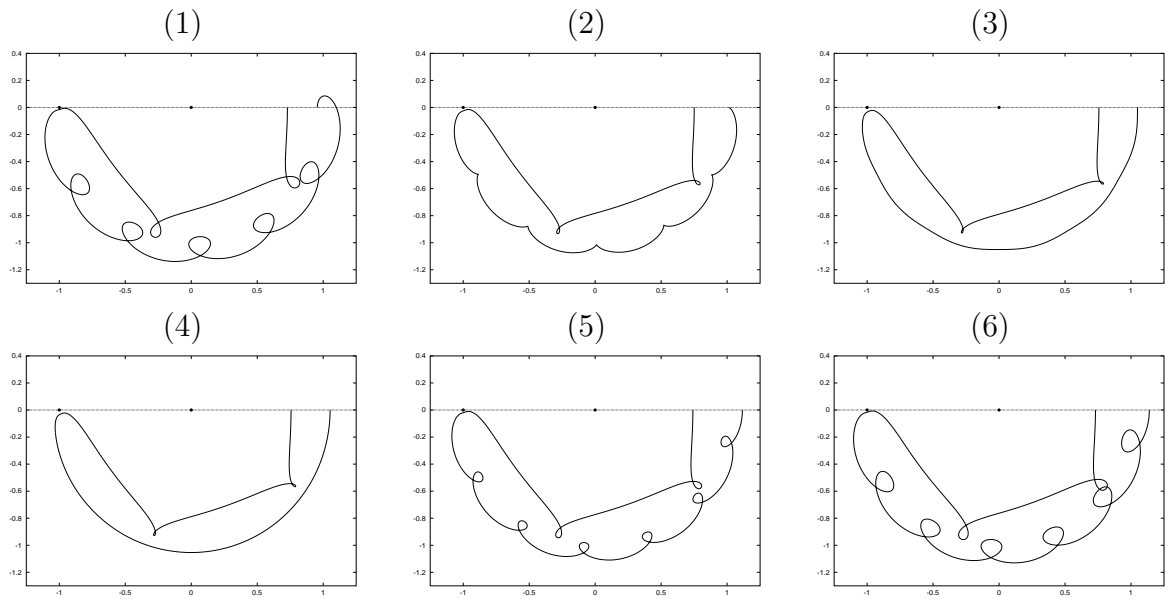


Figure 7: Samples of HPOs from family A ((x, y) projection). The numbering corresponds to the rhombus, with increasing x_0 , in Figure 6

crossings of the HPO with the horizontal axis (only two of them being orthogonal).

(iv) It is quite easy from Subsection 3.1 to describe the evolution of the main features

Figure 8: Samples of HPOs from family C ((x, y) projection).

related to the initial and final (at $t = T/2$) conditions along each family. In particular, we want to describe whether the particle is at a pericentre or an apocentre at $t = 0$ and the evolution of the sign of y'_0 . See Figures 6, 7 and 8 for orbits of family A and C as examples. With respect to the question of the initial condition being an apocentre or pericentre, it only depends on whether it is in a left or in a right branch. The left branch of each family is close to the corresponding upper and left semi-ellipse (generating family for $\mu = 0$) satisfying Equation (8). That means, from Figure 4, that the initial position point $(x_0, 0)$ of every HPO in a left branch corresponds to a pericentre of the approximating direct rotating ellipse. Analogously, the initial conditions in the right branches of the families correspond to an apocentre of the approximating ellipse. In both cases and for all the orbits computed, the sidereal velocity of the approximating ellipse is positive, this is, $y'_0 + x_0 \geq 0$, although the synodical velocity y'_0 can change its sign. Consider a family with a left branch. There is a particular x_0 for which the family is tangent to the ZVC, therefore $y'_0 = 0$ (see orbit (3) in Figure 7). From this value of x_0 downwards, $y'_0 > 0$ (see orbits (1) and (2) in Figure 7), while from this value onwards, $y'_0 < 0$, but the initial point still corresponds to a pericentre until the family crosses the skeleton. This fact can be observed also for the generating families (the upper left semi-ellipses are tangent to the ZVC before its intersection with the family of circular orbits, see Figure 4). At this point (when the family crosses the skeleton), there is an x_0 such that the approximating outer solution is circular (see orbits (4) in Figures 7 and 8). Then, as x_0 increases, we have the right branch of the family approximated by another upper and right semi-ellipse (generating family) given by (8), with a different semimajor axis a . Therefore the initial point takes place at an apocentre (of the corresponding rotating ellipse) all along the right branch.

Of course, the same comments apply to the curve given by the final points (x_f, C) with $(x_f, 0, 0, y'_f)$ at $t = T/2$ (see Figure 6 for such curves for families A and C). In Figures 7 and 8, we see that at the position point $(x_f, 0)$, the particle is always at the apocentre for family A and at the pericentre for family C. Let us finally remark that, looking at the characteristic curve (x_f, C) of families A and C, the two branches might seem to be the same, but they are not, with the maximum separation between both branches being close to the C_m value of the family.

Finally, we can describe the location of the initial condition x_0 with respect to the position of L_3 (at x_3). It is clear that in each generating family, for $a \geq 1$, there exists a value of C corresponding to a point in the upper left semi-ellipse for which $x_0 = 1$. Equivalently, for $\mu > 0$ and each family with a left branch, there is point (x_0, C) verifying $x_0 = x_3$. This is clearly observed in the evolution of x_0 in family A or C. The initial conditions in the right branches always satisfy $x_0 > x_3$, while the initial conditions in the left branches only satisfy $x_0 > x_3$ for values of C greater of a certain value (different for each family). With respect to the final conditions, in family A, $x_f < x_3$ only for values greater than another value of C , while in family C, $x_f < x_3$ always (see Figure 6).

- (v) Let us finally make two important remarks. On one hand, as $C_1 = 3.00895589$ and $C_3 = 3.00019998$, the region of HPOs explored is in a tiny neighbourhood of C_3 , say $C_3 - a, C_3 + b$, where $b > 0$ is small due to the C_1 value. On the other hand, there is no limitation, in principle, for $a > 0$, but as C decreases, the orbits become tremendously unstable and we have not computed them. Therefore, the question as to whether the characteristic curve of each family of HPOs is closed or not (as suggested from the closed ellipses of generating ellipses for $\mu = 0$) remains open for a future paper.

As we have just shown, it is clear that the two-body problem explains the behaviour of the characteristic curves of the continuous families of HPOs as well as many geometrical properties of each HPO. However, for any given HPO, what the two-body approximation does not explain is the intermediate piece of the solution between the outer and inner solutions, that is, when the returning point takes place. Of course, the dynamics of the returning point might be much more complicated (see Section 4). In fact, when C is close to, and less than, C_1 , there is a thin neck region given by the ZVC, that allows the path to pass from the outer region –where the outer solution lives– to the inner one –the oval shape region around the big primary m_1 , where there is the inner solution– (see Figure 1). Of course the small primary plays a key role there. But also, for any value of $C < C_1$, the invariant manifolds of the Lyapunov orbits associated with the collinear points L_1 and L_2 exist and play a role as well. See Section 4 (also [4] and [11]).

In addition to the description of the families of HPOs and some of their properties from the generating families for $\mu = 0$, we can derive other interesting features from the data obtained in the numerical computation of the families.

We now consider the (linear) stability of the computed HPOs. Given a periodic orbit

of period T , it is well known that the monodromy matrix M (the fundamental matrix of the linear variational system of differential equations along a periodic solution for $t = T$) has the eigenvalues $1, 1, \lambda_1, 1/\lambda_1$ and $s_p = \lambda_1 + 1/\lambda_1 = 2 - \text{tr}(M)$ is known as the stability parameter (see, for instance, [1], [13]). A periodic orbit is (linearly) stable if $|s_p| < 2$, and when the stability parameter equals 2 or -2 the orbit is called critical since families of the same period or doubling period respectively may bifurcate (see for instance [18] and [19]).

Regarding now the stability of the set of families of the computed HPOs, two common features appear along each family. First, when C along the family reaches the maximum value C_m , the stability curve crosses the line $s_p = 2$ as expected (see [13]). Second, when C varies along the family, there appears a tangency to the line $s_p = -2$ or even some transversal crossings to this line, so families of double period of HPOs may bifurcate. Therefore we may conclude that for any given family there is always one interval (or more) in the initial value x_0 for which the HPOs are stable although such intervals may be extremely thin (see [1] for details). Also, there are always bifurcation orbits where a family of the same or double period (depending on the value of s_p of this orbit) bifurcates.

Let us show an example of bifurcating families of double period. We consider a family with a tangential crossing with the line $s_p = -2$ and the associated value of C of this orbit. In Figure 9, top left, the curve (x_0, s_p) of such a family is shown. The bifurcating orbit with $s_p = -2$ is $x_0 = x_{0,bif}$ and $C = 3.0007512$. Now we fix this value of C and for a range of values of x_0 in an interval containing $x_{0,bif}$, we consider the orbit with this initial condition (y'_0 obtained from C) and the value of x'_f at the first cross of the orbit with the horizontal axis and the (x_0, x'_f) curve. This curve is shown in Figure 9, top middle. As expected, there is only one point such that $x'_f = 0$ that corresponds to the bifurcating HPO. However, if we decrease the C value slightly, and we compute the (x_0, x'_f) curve not at first, but at the second crossing, there appear three points with $x'_f = 0$ (see top right in the same Figure for $C = 3.0007506$): the one in the middle corresponds to the bifurcating HPO of simple period and the left and the right points correspond to two bifurcating HPOs of double period. One of the bifurcating HPO is plotted for $t \in [0, T/2]$ in Figure 9 (bottom left and a zoom in right). Therefore, we would obtain two new families of bifurcating double period HPOs (with four crossings in a period). We notice that we have not followed them, so these orbits do not appear in the diagrams shown in Figures 5 and 6.

3.3 Continuation of families of HPOs in the mass parameter

Naturally, once we have computed families of HPOs for a fixed and small $\mu_F = 0.0001$, we wonder about the continuation of the diagram of the characteristic curves of such families when varying μ . Of course an HPO may have many crossings with the x axis although only two of them will be orthogonal. This fact will be an inconvenient when we want to continue the families by varying the mass parameter μ . An easy way to perform the continuation would be simply to consider one family for μ_F and compute the new family for $\mu_N = \mu_F + \Delta\mu$ either by taking one point of the known family and making the continuation up to μ_N , and then from this new point, computing the new family for

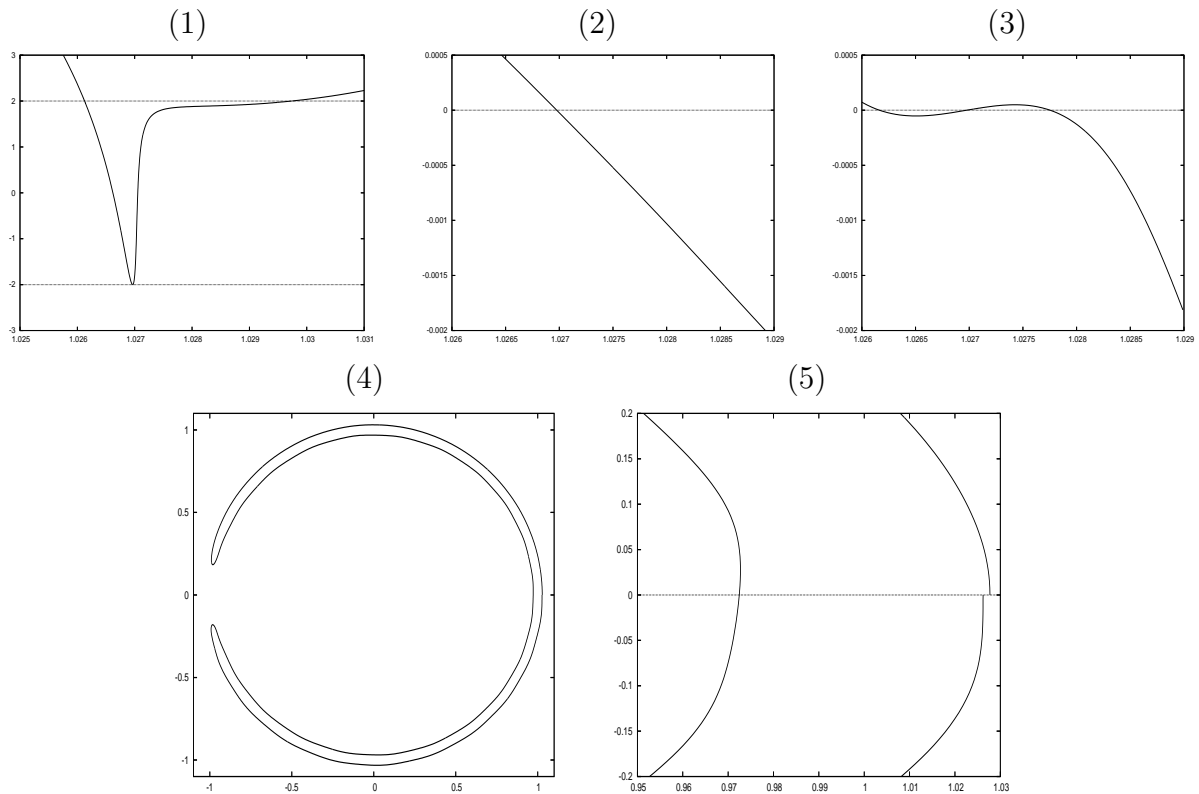


Figure 9: Example of a bifurcation family of double period for $\mu = 0.0001$. (1) Curve (x_0, s_p) of a family of HPOs with a bifurcation orbit with $s_p = -2$; (2) for $C = 3.0007512$ fixed (corresponding to the bifurcation orbit), the curve (x_0, x'_f) at first crossing; (3) for $C = 3.0007506$ fixed, (x_0, x'_f) curve at second crossing; (4) example of a bifurcating HPO of double period in the (x, y) plane for $t \in [0, T/2]$; (5) a detail of the HPO: not the first but the second crossing is orthogonal (at $t = T/2$) (this plot is not scaled in order to observe this fact).

μ_N fixed, or making the continuation of each point of the family from μ_F to μ_N . There would be no problems in such a continuation for $\mu_N < \mu_F$. However, the continuation in certain regions of the diagram is very sensitive in μ when μ goes onwards from μ_F .

To show this effect, let us restrict, when increasing μ , to the region of the diagram where the Jacobi constant is equal to $C = C_3$. First, let us compute for a given μ , the curve (x_0, x'_f) , where $(x_0, 0, 0, y'_0)$ is the initial condition of an orbit (with $y'_0 < 0$) and x'_f is the value of the velocity component x' at the first crossing of the orbit with the horizontal synodical axis, for x_0 increasing onwards from $x_3 + \delta$, $\delta > 0$ very small. Let us compare the obtained curves for increasing values of μ . For $\mu = 0.0001$, we see in Figure 10 top left, that many values of x_0 for which $x'_f = 0$ exist. Each of these values gives the initial condition (y'_0 obtained from the value C_3) of an HPO with two crossings with the horizontal axis in one period. We can also see many intervals for which there are jumps or discontinuities in the curve. In each one a value x_0 for which $x'_f = 0$ not at the first cross, but at the second one exists. This value corresponds to an orbit whose projection in the

(x, y) plane has a loop close to the first crossing (see Figure 11), and therefore such an x_0 corresponds to an HPO with 4 crossings with the $y = 0$ line in one period. However, we might say that the (x_0, x'_f) curve for $\mu = 0.0001$ is quite regular (in the sense of being an increasing sinus curve type). But when we slightly increase μ , for example $\mu = 0.00015$, a different behaviour is obtained for the corresponding (x_0, x'_f) curve (see Figure 10 top right). Although there are still values of x_0 such that $x'_f(x_0) = 0$, which correspond to HPOs with two crossings. For $\mu = 0.0005$ and the corresponding (x_0, x'_f) curve we remark that there are no HPOs with only two crossings in one period for any value x_0 in the interval $(x_3, 1.00024)$ (see Figure 10 bottom left). Thus, the number of intersections with the horizontal axis can change from one value of μ to another one, and this will be a problem when doing the continuation by varying the mass parameter. However, for bigger values of μ , we remark that we recover again the regular behaviour of the (x_0, x'_f) curve, although the whole curve moves up or down when varying μ . In Figure 12 we plot the curve (x_0, x'_f) at the first crossing for $\mu = 0.00697485$ (left), $\mu = 0.007$ (middle) and $\mu = 0.008$ (right). In the first case, there seems to be an infinite set of points with $x'_f = 0$ (this will be confirmed later, in Section 4), whereas for the other two values of μ we have just a finite one.

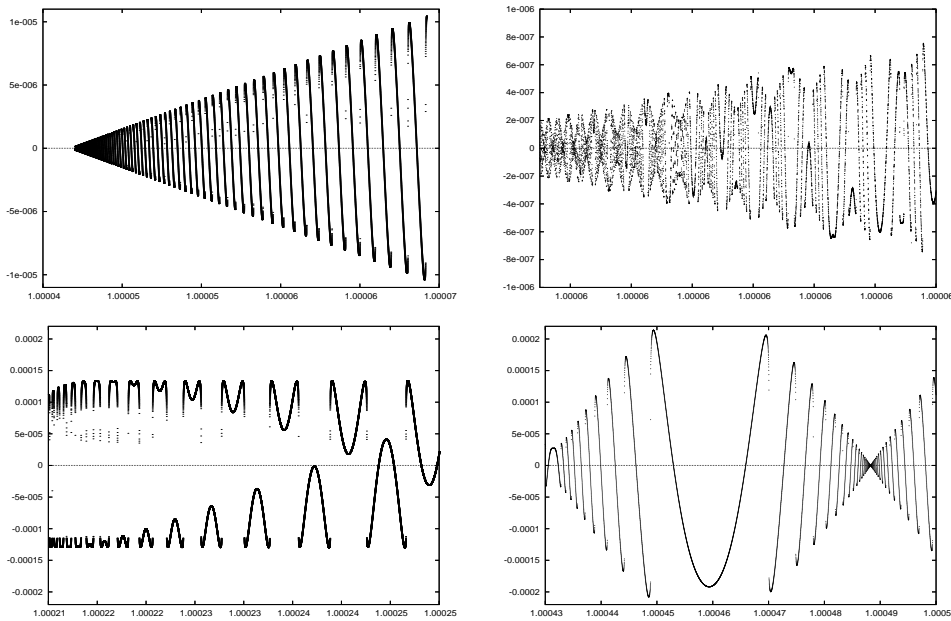


Figure 10: Curve (x_0, x'_f) for Jacobi constant $C = C_3$ and $\mu = 0.0001$ (top left), $\mu = 0.00015$ and $x_0 \in [1.0000627, 1.000064]$ (top right) and $\mu = 0.0005$ (bottom, left and right).

It is clear now that the obtained diagram of HPO for $\mu = 0.0001$ (Figure 6), will be rather different when the mass parameter increases. In Figure 13 the diagram of the characteristic curves in the (x_0, C) plane for $\mu = 0.008$ is shown. The families have been computed using the method explained in Subsection 3.2: continuing the families from the HPO obtained by fixing a value of C , and looking for orbits with $x'_f = 0$. When

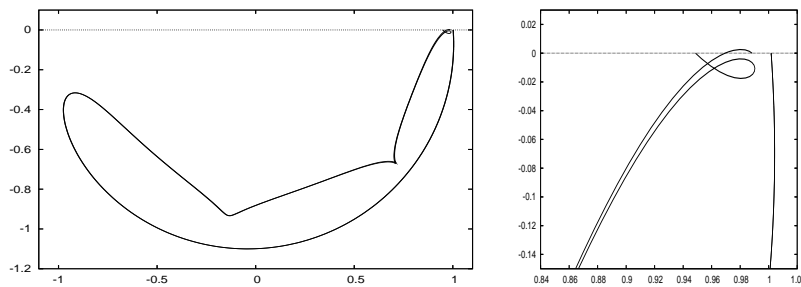


Figure 11: Left. Two horseshoe (non periodic) orbits with a loop close to the first crossing with the x axis (projection in the (x, y) plane). Right. Zoom.

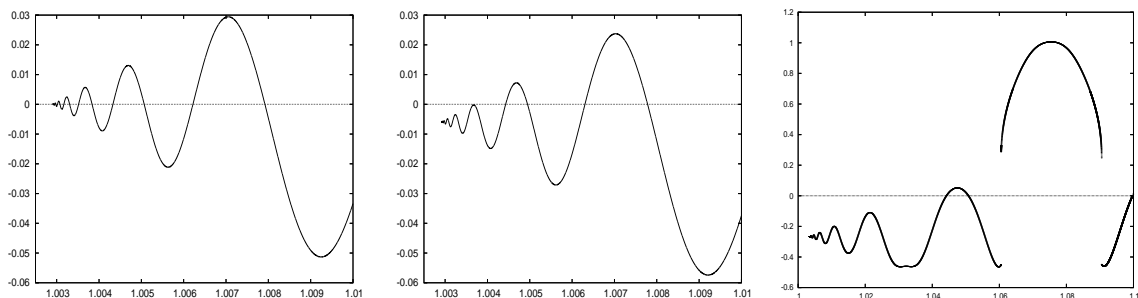


Figure 12: For $C = C_3$, curve (x_0, x'_f) at first crossing for $\mu = 0.00697485$ (left), $\mu = 0.007$ (middle) and $\mu = 0.008$ (right).

comparing both diagrams ($\mu = 0.0001$ and $\mu = 0.008$) we observe the following differences: first, as explained above and shown in Figure 12 right (curve (x_0, x'_f) for $C = C_3$), for the $\mu = 0.008$ case, there are not HPOs (with only two crossings) near L_3 . Second, the rigid structure of families organised in branches around the skeleton (see Figure 5) disappears completely when μ increases. Actually, the influence of the two body problem disappears as μ increases, but the small primary and the Lypaunov orbits around L_1 and L_2 play their role instead. For example, to find HPOs that enter the neighbourhood of the small primary is easier for $\mu = 0.008$ than for $\mu = 0.0001$, and the HPOs become more intricate, having several crossings with the x axis. In Figure 14 three HPOs for $\mu = 0.008$ are shown.

Thus, we can conclude that the continuation of the families of HPOs is very sensitive with respect to μ . The reasons for the differences in the diagrams of families for different values of μ depend on the behaviour of the invariant manifolds of L_3 , and the existence of homoclinic orbits to L_3 , as we will see in Section 4.

4 Horseshoe motion for $\mu \in (0, 1/2]$.

Our most ambitious goal in this Section is to analyse the existence of HPOs for any value of the mass parameter $\mu \in (0, 1/2]$ in an interval of values of C close to C_3 . Of course, a mechanism suitable to describe the HPOs for $\mu > 0$ and small (as explained in

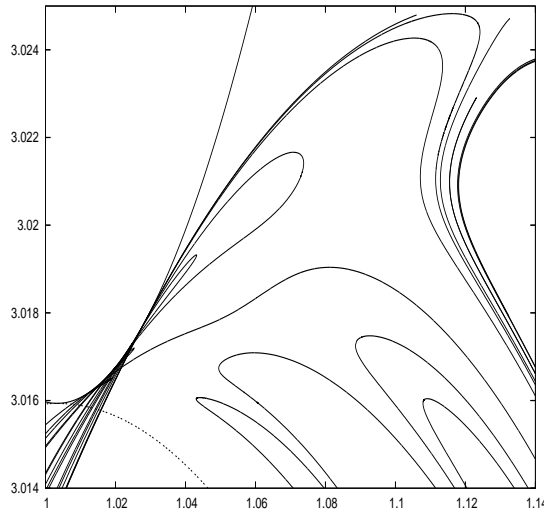


Figure 13: Characteristic curves of families of HPO for $\mu = 0.008$. The dotted curve on the bottom corresponds to the Lyapunov family around L_3 .

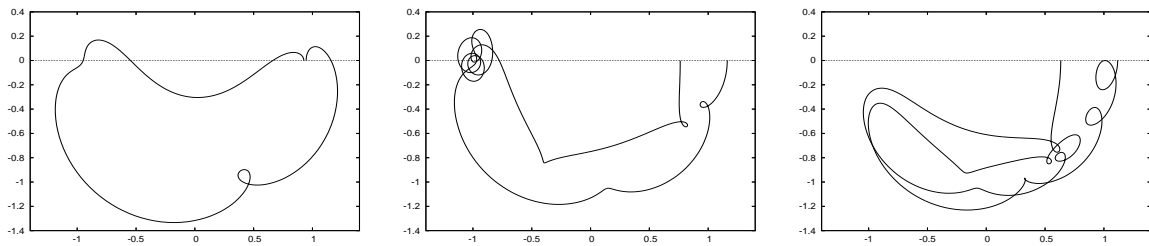


Figure 14: Samples of HPO for $\mu = 0.008$ and $C = 3.0000029162232198$, $x_0 = 0.9462538001607815$ (left), $C = 3.0128479526207705$, $x_0 = 1.162120446968716$ (middle) and $C = 3.0082900381403035$, $x_0 = 1.117289488220401$ (right).

Section 3), does not apply for any given value of μ . We are going to show that a natural mechanism that explains the existence of HPOs and the differences between the diagrams of the characteristic curves (of the families of HPOs) for different values of μ , relies on the behaviour of the one-dimensional manifolds of the collinear point L_3 .

We recall that to compute the two branches of the unstable manifold, $W_{L_3}^{u,i}$ $i = 1, 2$, we have taken as an initial condition $P_{L_3} + s \cdot v$, where s is a small quantity (usually 10^{-6}) positive or negative according to $i = 1, 2$ respectively, and v is the unit eigenvector associated to the eigenvalue $\lambda > 0$ of the Jacobian matrix of the vector field at L_3 . From this initial condition, we follow the invariant manifold numerically (integrating the system of ODEs) under the check test that along the integration the Jacobi constant values must be $C = C_3$.

Throughout this Section, two main ideas will play a role: (i) given $\mu > 0$, if the manifold $W_{L_3}^{u,i}$, $i = 1$ or 2 , has a first (or k -th) orthogonal crossing with the x axis, i.e. $y = x'_f = 0$, then (by symmetry (3)), the unstable and stable manifolds intersect giving rise to a homoclinic orbit which tends asymptotically, in forward and backward time, to

L_3 . For this μ value, we expect the existence of an infinite set of orbits approaching the homoclinic orbit (known as blue sky catastrophe phenomenon after Devaney [9], see also [14] and [15]). (ii) if in addition, the (stable or unstable) invariant manifold of L_3 has a horseshoe shape (this is, with the orthogonal crossing close to L_3) we may expect to have HPOs in a neighbourhood of it. So, along this Section, we will concentrate on the $C = C_3$ value, where the manifolds of L_3 exist.

First of all, we will apply these two ideas to answer the open question, described in Subsection 3.3, concerning the description of the diagram (of characteristic curves of families of HPOs) for different values of μ at C_3 . This is done in Subsection 4.1, where an exploration for selected values of μ , is done.

Next, we focuss our attention on the following natural question: for which values of μ do the invariant manifolds of L_3 (i) have a horseshoe shape? (ii) become homoclinic orbits? Thus, a systematic exploration of the shape of the invariant manifolds of L_3 is carried out for all values of $\mu \in (0, 1/2]$. The values of μ for which there is a homoclinic connection are analysed as well. We will see that, for $\mu \in (0, 0.01174]$ two different sequences of values of μ , $\mu_{n,homo,1}$ and $\mu_{n,homo,2}$ exist, both tending to 0 as $n \rightarrow \infty$, for which an homoclinic orbit to L_3 exists. For each value of μ in $\mu_{n,homo,1}$, the homoclinic orbit has only one crossing (the orthogonal one) with the x axis, whereas for μ in $\mu_{n,homo,2}$, the homoclinic orbit has a loop (so there are three crossings with the x axis, the second one being orthogonal). This is explained in Subsection 4.2.

For $\mu > 0.01174$, the manifolds enter in the neighbourhood of the small primary, where the presence of the other two equilibrium points L_1 and L_2 as well as the small primary play a role. For such values of μ , we obtain either horseshoe invariant manifolds which describe a path close to the small primary or even collide with it, or manifolds which have no horseshoe shape at all. This is explained in Subsection 4.3.

Finally, in Subsection 4.4 we show how the phenomenon of double homoclinic orbits bifurcation around each $\mu_{n,homo,i}$, for $i = 1, 2$ takes place.

4.1 Invariant manifolds of L_3 when varying μ

From the invariant manifolds of L_3 it is now easy to explain the plots in Figure 10 and 12. First we plot the (x, y) projection of the unstable manifold $W_{L_3}^{u,1}$ for $\mu = 0.0001$ (Figure 15 top and bottom left). The invariant manifold has a simple horseshoe shape and is almost a homoclinic orbit. The homoclinic connection occurs for $\mu = 0.00010001$, for which an infinite sequence of HPOs approaching the homoclinic orbit exist (this is known as blue sky catastrophe). This fact explains the infinite sequence of values x_0 (of the initial conditions of HPO) accumulating to x_3 which we can see in Figure 10 top left. But as μ increases slightly from 0.0001, we can see how the loops close to the first crossing with the x axis appear and that the width of the loops grows rapidly in μ (Figure 15 top middle). It is this width of the loops that has consequences on the dynamics of the orbits and, from Figure 15 top middle, it is easy to understand that small variations of the value of μ gives invariant manifolds with the orthogonal crossing at the first intersection with the horizontal axis or at the second one. More precisely, for $\mu = 0.0001$ the width of the loops is very small and therefore it has no effects on the (x_0, x'_f) curve (which has regular

behaviour as shown in Figure 10 top left), whereas for $\mu = 0.0005$, due to the loops that appear in the invariant manifolds (Figure 15 top middle) the HPOs for values x_0 near x_3 have more than two crossings (thus, the curve $x'_f(x_0)$ at the first cross does not intersect the horizontal axis, see Figure 10 bottom left).

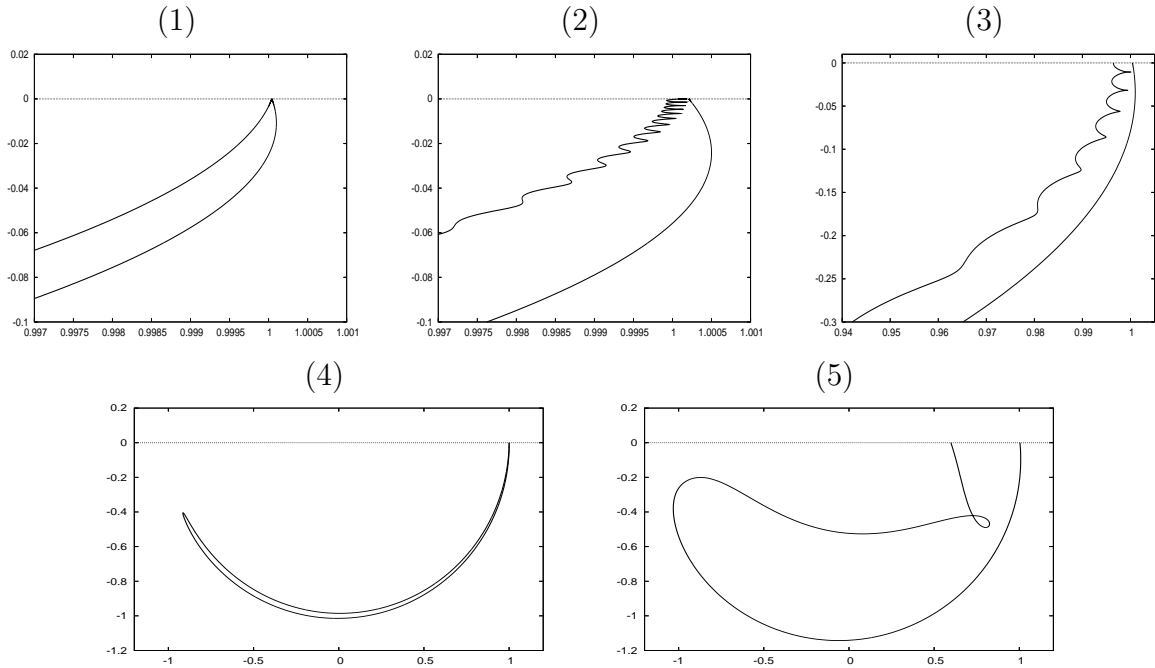


Figure 15: Projection (x, y) of the manifold $W_{L_3}^{u,1}$ until the first cross with the horizontal axis. Top. Zoom near L_3 for: (1) $\mu = 0.0001$, (2) $\mu = 0.0005$, (3) $\mu = 0.001$. In order to see the differences between them, these plots are not scaled. Bottom: (4) $\mu = 0.0001$, (5) $\mu = 0.008$.

On the other hand, the loops may also produce the existence of an infinite set of initial conditions of HPO accumulating to a certain x_0 far from x_3 . This is the case for $\mu = 0.0005$: we plot the curve (x_0, x'_f) for $x_0 > x_3$ and we concentrate on the interval $x_0 \in [1.00043, 1.0005]$ (Figure 10 bottom right). Near the value $x_0 = 1.00048826$ there seems to exist an infinite number of HPO with only two crossings, but in fact only a finite number exists (as a zoom exploration reveals). If we compute the manifold $W_{L_3}^{u,2}$, we observe that the first crossing (almost orthogonal) takes place at $x_f = 1.000489376$, $x'_f = 8.175 \cdot 10^{-6}$. Of course the case $x'_f = 0$ would imply a homoclinic orbit to L_3 and the existence of an infinite set of HPO tending to it. In fact, for $\mu = 0.0005$, we would expect a homoclinic orbit to the Lyapunov orbit around L_3 for a suitable value of $C < C_3$ and very close to C_3 .

We finally remark that this loop shape of the manifolds of L_3 disappears as μ increases, see Figure 15 top and bottom right. So we have the simple plots in Figure 12. The infinity of HPOs for $\mu = 0.00697485$ (points with the $x'_f(x_0) = 0$ in the left plot in the same Figure) with the corresponding initial x_0 tending to x_3 , is just a direct consequence of the homoclinic (horseshoe shape) orbit to L_3 for this value of μ (again a blue sky catastrophe).

Instead, for a μ slightly different, $\mu = 0.007$ and also $\mu = 0.008$, Figure 12 centre and right), the invariant manifolds describe a simple horseshoe shape but are not homoclinic, and therefore, only a finite number of HPOs appears. This is the reason for the gap at $C = C_3$ in the diagram of characteristic curves for $\mu = 0.008$ (Fig. 13) compared to the diagram for $\mu = 0.0001$ (Fig. 5 and 6 left).

Therefore, in summary, we have shown that, although the plots of the manifolds are qualitatively similar, the loops have relevant dynamical consequences for the diagram of characteristic curves of HPOs at $C = C_3$.

4.2 Homoclinic orbits to L_3 when varying μ

Motivated by the previous Subsection, we proceed to a systematic exploration, for $\mu \in (0, 1/2]$, of the behaviour of the unstable manifolds of L_3 (a similar analysis follows for the stable ones). Our aim is to explore for which values of $\mu \in (0, 1/2]$ the manifolds have a horseshoe shape and are homoclinic to L_3 . Of course, for each such μ , the dynamics concerning HPO will be similar to the one described in the previous section.

Therefore, we compute $W_{L_3}^{u,1}$ for each value of $\mu > 0$ and we keep the x and x' values at the k -th crossing with the x axis, $y = 0$, denoted from now on as $x_{f,k}$ and $x'_{f,k}$. Firstly, we will concentrate on the analysis of the behaviour of the invariant manifolds from L_3 at the *first* crossing, ($k = 1$), with the x axis. Furthermore, some aspects of the dynamics that have to do with other crossings and that will appear in a quite natural way will be also remarked on.

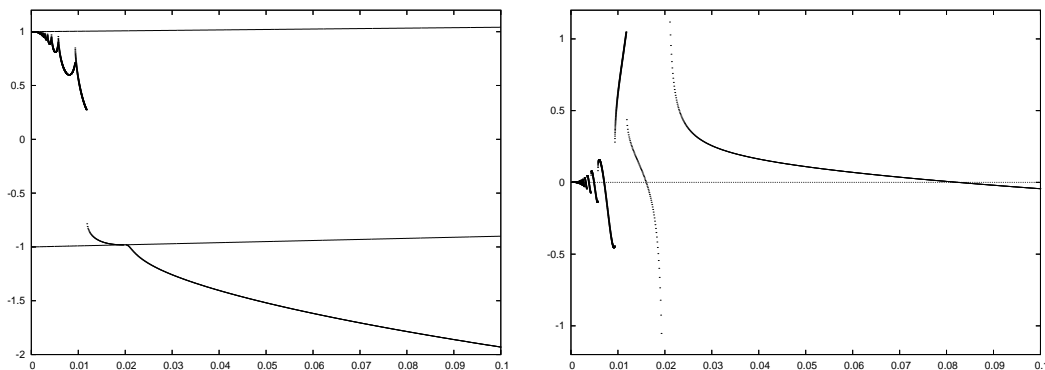


Figure 16: Left: Curve $x_f(\mu)$ (left) and $x'_f(\mu)$ (right) at the first crossing. In the figure on the left, the position of L_3 (x_3) and the small primary for each value of μ are also plotted (see the text for details).

We plot in Figure 16 the $(\mu, x_{f,1})$ and the $(\mu, x'_{f,1})$ curves and the positions of L_3 and the small primary $(\mu, \mu - 1)$ as well. From these plots we have the following results related to horseshoe motion.

- (i) When $0 < \mu \leq 0.01174$ the invariant manifold associated with each value of μ has a horseshoe shape. This has been numerically checked through the condition that the manifold crosses the $x = 0$, $y < 0$ semi-axis twice –at least– but does not cross

the $x = 0, y > 0$ semi-axis before the manifold crosses $y = 0$ at $x > 0$. Furthermore, the first crossing with the horizontal axis at $x > 0$ takes place with $x_{f,1}$ close to L_3 and on its left (see Figure 16 left). For $\mu > 0.01174$ the invariant manifold crosses the $y = 0$ axis for $x < 0$ and the influence of the small primary must be taken into account. We discuss this fact in the Subsection 4.3.

- (ii) We also remark that when $0 < \mu \leq 0.01174$, there are infinitely many values of μ such that $x'_{f,1} = 0$ (see Figure 16 right), each one corresponding to a horseshoe homoclinic orbit to L_3 with an orthogonal crossing at the first cross with $y = 0$. Actually, Font ([10]) computed some values of μ tending to 0 for which there is a homoclinic connection to L_3 . Let us denote this infinity of values μ as $\mu_{n,homo,1}$ such that when $n \rightarrow \infty$, $\mu_{n,homo,1} \rightarrow 0$.
- (iii) In this range of μ values, each ‘sharp’ point in the $(\mu, x_{f,1})$ curve is associated to a jump or discontinuity in the $(\mu, x'_{f,1})$ curve. For these values of μ the projection in the (x, y) plane of the invariant manifold has a loop (see also Figure 11). Therefore the values of $x_{f,2}$ and $x'_{f,2}$ at the second crossing must be taken into account. As discussed in Section 3, for each discontinuity in the (x_f, x'_f) curve, there is a nearby horseshoe homoclinic orbit such that the second crossing (the orthogonal one) takes place at the half loop –in the (x, y) plane– (see Figure 19 bottom). Since there is another infinity of such discontinuities in $x'_{f,1}$, that means there is another infinity of horseshoe homoclinic orbits each of them with a loop. Let us denote this sequence as $\mu_{n,homo,2}$ (also $\mu_{n,homo,2} \rightarrow 0$).

In conclusion, we have found two sequence of μ values tending to zero such that for each value a homoclinic connection to L_3 exists. For each such value, the blue sky catastrophe occurs and an infinity of periodic orbits (horseshoe-shaped like the homoclinic orbits) exist. Clearly, for values of μ close to $\mu_{n,homo,i}$, $i = 1, 2$, HPOs still survive and can be found.

4.3 Collision manifolds and influence of L_2

We have just described the evolution of the first crossing curve $x_{f,1}(\mu)$ for $\mu \in (0, 0.01174)$. Let us go on describing the behaviour of this curve for $\mu > 0.01174$ (see Figure 16).

There is another discontinuity in both curves $x_{f,1}(\mu)$ and $x'_{f,1}(\mu)$ which has nothing to do with loops. This corresponds to the jump in x_f observed for $\mu = 0.01175$. It takes place because there is a tangency with the negative x axis. For increasing values of μ the invariant manifold is still horseshoe shaped although it invades the $x < 0, y > 0$ region. Therefore, not the first but the third crossing (at least) with the y axis will be meaningful for horseshoe motion. However, keeping track only of the first crossing $x_f < 0$ and for values of μ after the tangency, we find the value $\mu_{homo,1} = 0.0159375$, for which the manifold is a homoclinic orbit to L_3 , and the value $\mu_{col,1} = 0.02004225$, for which the unstable manifold collides with the small primary at the first crossing. See Figure 16 right, where the value $\mu_{col,1}$ corresponds to the last intersection of the curve with the horizontal axis. We have used Levi-Civita coordinates (see [23]) in order to regularise

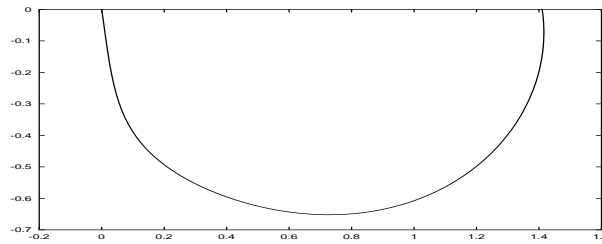


Figure 17: For $\mu_{col,1} = 0.02004225$ the unstable manifold of L_3 collides with the small primary (Levi-Civita position coordinates).

the binary collision between the particle and the small primary. In Figure 17 we show this manifold in the position Levi-Civita coordinates (u, v) (the collision corresponds to the origin). After the collision, when μ increases, the x_f value (still at the first crossing with $y = 0$) keeps decreasing on the left of the position of the small primary. In fact, for $\mu \geq \mu_{homo,1}$ the unstable manifold $W_{L_3}^{u,1}$ does not have a horseshoe shape anymore.

At this point, let us comment in more detail on what happens when the invariant manifold visits the $x < 0, y > 0$ region when μ varies in the interval $(0.01175, \mu_{col,1})$. Actually, since only the first crossing in the curve $(\mu, x'_f(\mu))$ is considered in Figure 16, this plot hides that the shape of the manifold of L_3 is more intricate. As stated above, the invariant manifold for $\mu > 0.01175$ crosses the $y = 0$ axis near the small primary and as μ increases the Lyapunov orbit around L_2 and the small primary play a role now. We have followed the manifold for up to seven crossings with the x axis, for varying μ , and our conclusion is that the following different behaviours of the invariant manifold take place: a trajectory surrounding the small primary and the Lyapunov orbit around L_1 or L_2 that does have a horseshoe shape (see Figure 18 top left and bottom right) or does not (see Figure 18 top right and bottom left). Furthermore, we observe that for a suitable value of μ a collision invariant manifold with the small primary exists (after a certain number of crossings with the x axis greater than one).

So we can conclude that the dynamics of the unstable manifold $W_{L_3}^{u,1}$ becomes very rich when m_2 and the Lyapunov orbit of L_2 are taken into account. A systematic analysis of such dynamics (considering also the influence of the Lyapunov orbits around L_1 and L_2), for any $\mu \in (0, 1/2]$ and for a given number of crossings (greater than two), remains for future work.

4.4 Double homoclinic bifurcation

Up to now, we have been describing the *simple* horseshoe manifolds of L_3 , in the sense that they surround L_4 and L_5 just *once*. However a more detailed numerical exploration reveals that **bifurcation** of *double period* homoclinic orbits (**surrounding twice L_4 and L_5**) appear, although the word ‘period’ does not make sense since a homoclinic orbit has, say, an *infinite* period. But the nomenclature recalls what happens in the periodic orbits context. From now on we will call it the double homoclinic orbit.

To show this phenomenon, let us now consider one of the values $\mu_{n,homo,i}$ (described in Subsection 4.2), for a *fixed* n and $i = 1$ or 2 . In particular, we have taken $\mu_{n,homo,1} =$

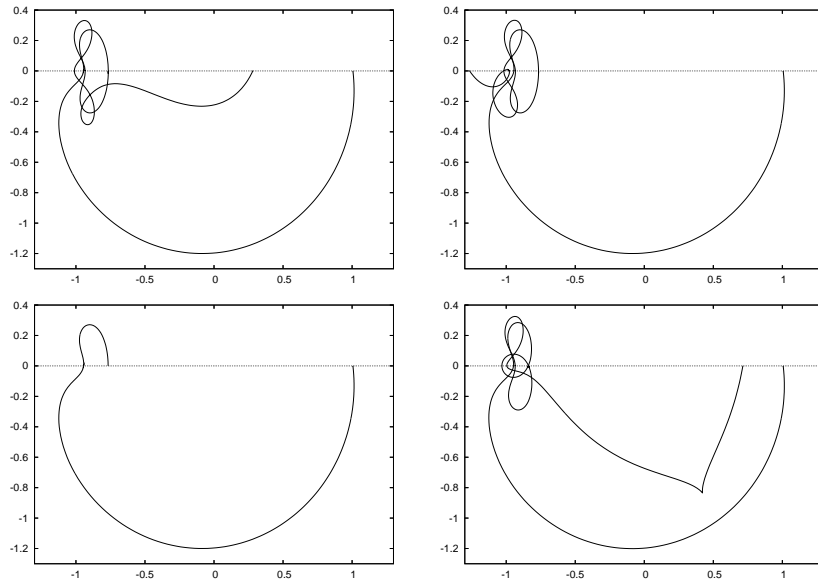


Figure 18: $W_{L_3}^{u,1}$ in the (x, y) plane for $\mu = 0.0145642$ (top left), $\mu = 0.01456344$ (top right), $\mu = 0.0145655$ (bottom left), $\mu = 0.0146968$ (bottom right). See the text for details.

0.0037258 and $\mu_{n,homo,2} = 0.0041976$. We have computed both $x'_{f,1}(\mu)$ and $x'_{f,2}(\mu)$ curves for the interval $\mu \in [0.0035, 0.0044]$ that contain both values $\mu_{n,homo,1}$ and $\mu_{n,homo,2}$. The interest in the curve $x'_{f,2}(\mu)$ is precisely to show the double homoclinic orbits. We consider a neighbourhood of $\mu_{n,homo,1}$ and one of $\mu_{n,homo,2}$ separately.

- (i) Let us concentrate first on the neighbourhood $I_1 = [0.0035, 0.004]$, which has $\mu_{n,homo,1} = 0.0037258$. In Figure 19 top, the curves $x_{f,1}(\mu)$ and $x_{f,2}(\mu)$ as well as $x'_{f,1}(\mu)$ and $x'_{f,2}(\mu)$ are represented (on the left, all the curves in the interval I_1 are plotted, while on the right, only the curves $x'_{f,i}(\mu)$, $i = 1, 2$ in a wide interval are shown). We can see that the first crossing is always close to and less than the position of L_3 , that is $x_{f,1} < x_3$. However, the second crossing $x_{f,2}(\mu) > x_3$. We also remark that whereas $\mu = \mu_{n,homo,1}$ is the unique value for which $x'_{f,1}(\mu) = 0$ in I_1 , we have infinite values of μ (on the left and right of $\mu_{n,homo,1}$) such that $x'_{f,2}(\mu) = 0$. Therefore, there are two sequences of values of μ , $\mu_{n,homo,1}^{m,2} < \mu_{n,homo,1}$, $\mu_{n,homo,1}^{m',2} > \mu_{n,homo,1}$ such that

$$\lim_{m, m' \rightarrow \infty} \mu_{n,homo,1}^{m, m', 2} = \mu_{n,homo,1},$$

and for each value of each sequence the invariant unstable manifold of L_3 becomes a homoclinic orbit to L_3 .

The geometric behaviour of such manifolds is the following: the horseshoe homoclinic manifold for $\mu_{n,homo,1}$ surrounds only once the points L_4 and L_5 in the (x, y) plane (see Figure 19 middle right). However, the horseshoe homoclinic manifolds

for $\mu_{n,homo,1}^{m,m',2}$ have their orthogonal crossing at the second one with $x_{f,i} > x_3$ once they have surrounded *both* L_4 and L_5 (see Figure 19 middle left). Thus, the whole homoclinic manifold surrounds the points L_4 and L_5 *twice*.

- (ii) In a similar way as discussed in Subsection 4.2, the infinity of jumps in the $x'_{f,2}(\mu)$ curve (see Figure 19 top), correspond to values of μ (on both sides of $\mu_{n,homo,1}$) for which a loop near the second crossing appears. Therefore, $x'_{f,3}(\mu) = 0$ at a half loop. Again we can conclude that there are two more sequences $\mu_{n,homo,1}^{m,3} < \mu_{n,homo,1}$, and $\mu_{n,homo,1}^{m',3} > \mu_{n,homo,1}$ such that

$$\lim_{m,m' \rightarrow \infty} \mu_{n,homo,1}^{m,m',3} = \mu_{n,homo,1},$$

and for each value of each sequence the invariant unstable manifold of L_3 becomes a homoclinic orbit to L_3 . The geometric behaviour of these homoclinic orbits are similar to the homoclinic orbits for $\mu_{n,homo,1}^{m,m',2}$ in the sense that the whole orbit surround L_4 and L_5 *twice*.

- (iii) Let us consider the interval $I_2 = [0.004, 0.0044]$ where the value $\mu_{n,homo,2} = 0.0041976$, for a fixed n , belongs to (see Figure 19 bottom). We also compute the curves $x_{f,1}(\mu)$, $x_{f,2}(\mu)$, $x'_{f,1}(\mu)$ and $x'_{f,2}(\mu)$ (see Figure 19 top). In this case there are four *finite* sets of values of μ for which the function $x'_{f,2}(\mu)$ has a zero or a jump discontinuity. As in the previous items, each of these values corresponds to a homoclinic orbit with a second or third crossing (the orthogonal one) on the right side of L_3 . But now, only a finite set is observed. This is due to the fact that, for μ close to $\mu_{n,homo,2}$, a loop intersecting the horizontal axis near the first crossing of the manifold appears. When this happens, not the second and the third, but the fourth and the fifth crossings (which will take place on the right side of L_3) should be taken into account.

This illustrates that the loops affect the number of crossings considered when studying the homoclinic connections.

The dynamical consequence of such double homoclinic orbits is that for each value of μ for which there is a double homoclinic orbit, there will exist an infinity of HPOs enclosing the points L_4 and L_5 *twice*, and tending to the homoclinic connection.

Finally, we remark that the two patterns just described also take place for any $\mu_{n,homo,i} \in (0, 0.01174)$, $i = 1, 2$, and $n \in \mathbb{N}$. See for instance Figure 19 top right, where only the curves $x'_{f,1}(\mu)$ and $x'_{f,2}(\mu)$ are plotted in the interval $\mu \in (0, 0.05)$. As we can see, the same patterns of crossings with $x'_f = 0$ described in detail in Figure 19 top left (the bottom part of the plot) repeat again and again when varying μ in Figure 19 top right.

5 Conclusions

We have analysed the horseshoe motion as a particular kind of motion in the RTBP. On the one hand, we show that the families of horseshoe periodic orbits for $\mu > 0$ and

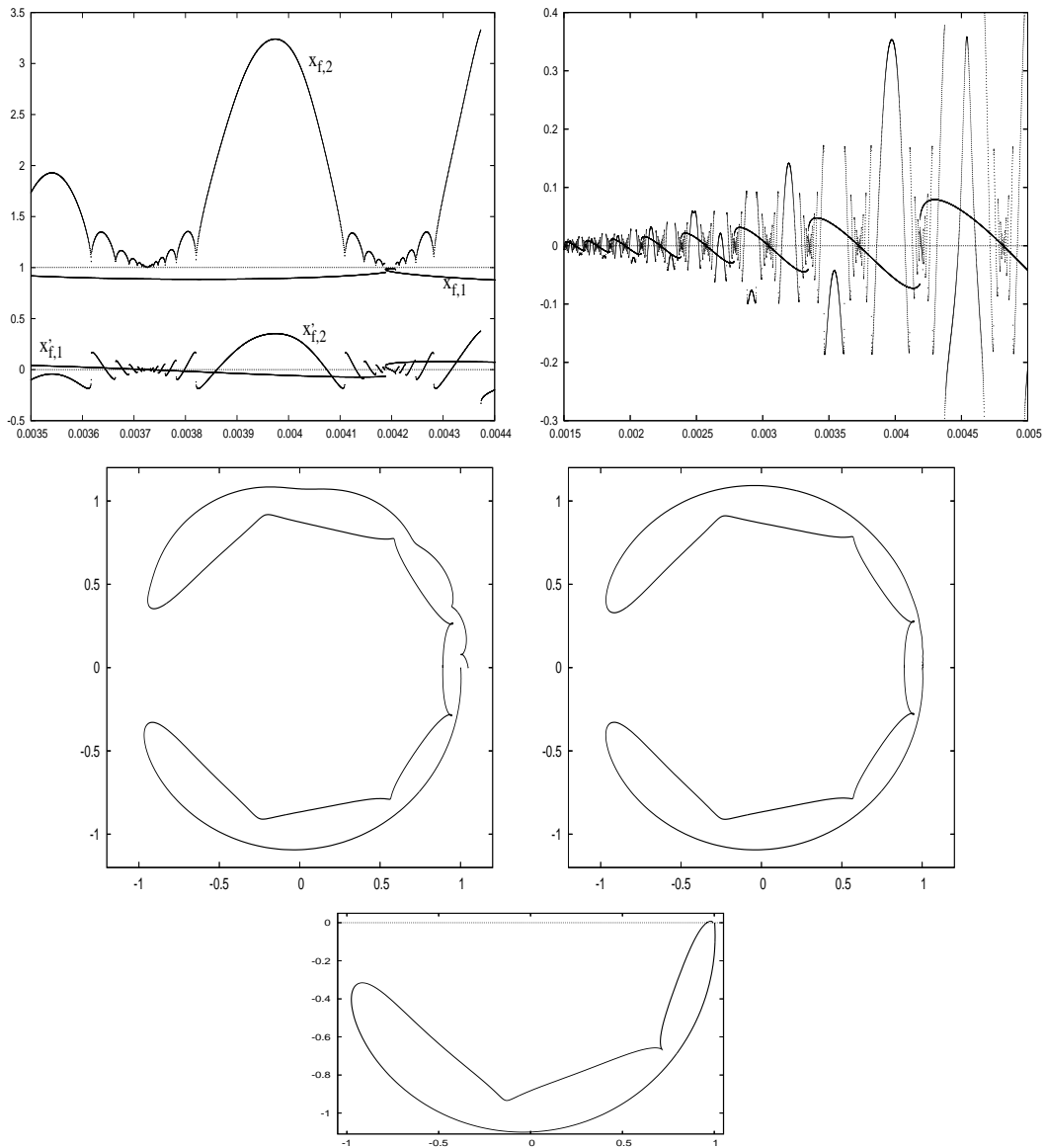


Figure 19: Top left. For n fixed, curves $x_{f,1}(\mu)$, $x_{f,2}(\mu)$, $x'_{f,1}(\mu)$ and $x'_{f,2}(\mu)$ around $\mu_{n,homo,1} = 0.0037258$ and around $\mu_{n,homo,2} = 0.0041976$. Curve $x_3(\mu)$ is also plotted. Top right. Curves $x'_{f,1}(\mu)$ and $x'_{f,2}(\mu)$. Middle. *Double* homoclinic invariant manifold $-(x, y)$ projection– for μ close to $\mu_{n,homo,1}$ (left); whole homoclinic manifold for $\mu_{n,homo,1}$ (right). Bottom. Homoclinic manifold for $\mu_{n,homo,2}$ with the orthogonal crossing at half loop.

small are closely related to the generating families of periodic orbits of the two-body problem. On the other hand, such horseshoe motion is closely related to the behaviour of the equilibrium point L_3 and its invariant stable and unstable manifolds. A systematic exploration for any μ has been carried out and turns out to be very useful in order to obtain results about the homoclinic behaviour of the manifolds as well as the horseshoe periodic orbits near them.

Acknowledgements

This research has been supported by the Spanish CICYT grant BFM2003–09504–C02–01 and the Catalan CIRIT grant 2001SGR–70.

References

- [1] E. Barrabés and S. Mikkola. Families of periodic horseshoe orbits in the restricted three-body problem. *Astron. Astrophys.*, 432:1115–1129, 2005.
- [2] E. Belbruno, J. Llibre and M. Ollé. On the families of periodic orbits which bifurcate from the circular Sitnikov motions. *Cel. Mech. and Dyn. Astron.*, 60: 99-129, 1994.
- [3] R. Brassier, K.A. Innanen, M. Connors, D. Veillet, P. Wiegert, S. Mikkola, and P.W. Chodas. Transient co-orbital asteroids. *Icarus*, 171(1):102–109, September 2004.
- [4] E. Canalias and J. Masdemont. Homoclinic and heteroclinic transfer trajectories between Lyapunov orbits in the Sun-Earth and Earth-Moon systems. *Preprint*, 2005.
- [5] M. Connors, P. Chodas, S. Mikkola, P. Wiegert, C. Veillet, and K. Innanen. Discovery of an asteroid and quasi-satellite in an earth-like horseshoe orbit. *Meteoritics & Planetary Science*, 37:1435–1441, 2002.
- [6] Josep M. Cors and Glen R. Hall. Coorbital periodic orbits in the three body problem. *SIAM J. Appl. Dyn. Syst.*, 2(2):219–237 (electronic), 2003.
- [7] Stanley F. Dermott and Carl D. Murray. The dynamics of tadpole and horseshoe orbits. i. theory. *Icarus*, (48):1–11, 1981.
- [8] Stanley F. Dermott and Carl D. Murray. The dynamics of tadpole and horseshoe orbits. ii. the coorbital satellites of saturn. *Icarus*, (48):12–22, 1981.
- [9] R. Devaney. Blue sky catastrophes in reversible and hamiltonian systems. *Ind. Univ. Math.*, 26:247–263, 1977.
- [10] J. Font. The role of homoclinic and heteroclinic orbits in two-degrees of freedom Hamiltonian systems. *Ph. D. Thesis*, Barcelona University, 1999.
- [11] G. Gómez, W. S. Koon, M. W. Lo, J. E. Marsden, J. Masdemont, S.D. Ross. Connecting orbits and invariant manifolds in the spatial restricted three-body problem. *Nonlinearity*, 17:1571–1606, 2004.
- [12] M. Hénon and M. Guyot. Stability of periodic orbits in the restricted problem. *Periodic Orbits, Stability and Resonances*, *G.E.O. Giacaglia (ed.)*, pages 349–374, 1970.

- [13] M. Hénon. Exploration numérique du problème restreint. *Ann. Astr.*, 28:992–1007, 1965.
- [14] J. Henrard. Proof of a conjecture of E. Strömberg. *Cel. Mech. and Dyn. Astron.*, 7:449–457, 1973.
- [15] J. Henrard and J. F. Navarro. Families of periodic orbits emanating from homoclinic orbits in the restricted problem of three bodies. *Cel. Mech. and Dyn. Astron.*, 89:285–304, 2004.
- [16] J. Llibre, M. Ollé. Horseshoe periodic orbits in the Restricted three-body problem, *New advances in celestial mechanics and Hamiltonian systems (HAMSYS-2001)*, Ed: J. Delgado, E. Lacomba, J. Llibre, E. Perez Chavela. *Kluwer Academic. Plenum Pub. New York*, 2004, pp 137–152.
- [17] J. Llibre, M. Ollé. The motion of Saturn coorbital satellites in the restricted three-body problem, *Astron. Astrophys.*, 378: 1087–1099, 2001.
- [18] M. Ollé and J.R. Pacha. The 3d elliptic RTBP: periodic orbits which bifurcate from limiting restricted problems: complex instability. *Astron. Astrophys.*, 351:1149–1164, 1999.
- [19] M. Ollé, J. R. Pacha, J. Villanueva. Motion close to the Hopf bifurcation of the vertical family of periodic orbits of L_4 . *Cel. mech. and Dyn. Astron.* 90: 89–109, 2004.
- [20] J. M. Petit and M. Hénon. Satellite encounters. *Icarus* 66: 536–556, 1986.
- [21] C. Simó. Effective computations in celestial mechanics and astrodynamics. In V. V. Rumyantsev and A. V. Karapetyan (ed.), *Modern Methods of Analytical Mechanics and Their Applications*, vol. 37 of CISM Courses and lectures, Springer Verlag, 1998.
- [22] F. Spirig, J. Waldvogel. The three-body problem with two small masses: a singular-perturbation approach to the problem of Saturn’s coorbiting satellites. *Stability of the solar system and its minor and Artificial Bodies*, ed. V. Szebehely (Reidel), pp. 53–64, 1985.
- [23] V. Szebehely. *Theory of orbits*. Academic Press, 1967.
- [24] J. Waldvogel, F. Spirig. Co-orbital satellites and Hill’s lunar problem. *Long-Term dynamical behaviour of natural and artificial N-body systems*, ed. A. E. Roy (Kluwer Acad. Pub.), pp. 223–236, 1988.